Superscaling of non-quasielastic electron-nucleus scattering

C. Maieron,[1] J.E. Amaro,[2] M.B. Barbaro,[3] J.A. Caballero,[4] T.W. Donnelly,[5] and C. F. Williamson[5]

[1]*Dipartimento di Fisica, Università del Salento and INFN, Sezione di Lecce, Via Arnesano, 73100 Lecce, ITALY*

[2]*Departamento de Física Atómica, Molecular y Nuclear, Universidad de Granada, 18071 Granada, SPAIN*

[3]*Dipartimento di Fisica Teorica, Università di Torino and INFN, Sezione di Torino, Via P. Giuria 1, 10125 Torino, ITALY*

[4]*Departamento de Física Atómica, Molecular y Nuclear, Universidad de Sevilla, Apdo. 1065, E-41080 Sevilla, SPAIN*

[5]*Center for Theoretical Physics, Laboratory for Nuclear Science and Department of Physics, Massachusetts Institute of Technology, Cambridge, MA 02139, USA*

(Dated: December 27, 2010)

Abstract

The present study is focused on the superscaling behavior of electron-nucleus cross sections in the region lying above the quasielastic peak, especially the region dominated by electroexcitation of the Δ. Non-quasielastic cross sections are obtained from all available high-quality data for ^{12}C by subtracting effective quasielastic cross sections based on the superscaling hypothesis. These residuals are then compared with results obtained within a scaling-based extension of the relativistic Fermi gas model, including an investigation of violations of scaling of the first kind in the region above the quasielastic peak. A way potentially to isolate effects related to meson-exchange currents by subtracting both impulsive quasielastic and impulsive inelastic contributions from the experimental cross sections is also presented.

PACS numbers: 25.30.Fj, 24.10.Jv, 13.60.Hb

I. INTRODUCTION

In recent years scaling [1, 2] and superscaling [3, 4] properties of electron-nucleus scattering have been studied in great detail. A first line of investigation has been focused on the behavior of experimental data and on the construction from them of suitable phenomenological models for lepton-nucleus scattering [3, 4, 5, 6, 7, 8]. A second line, developed in parallel to the first, has instead been focused on more theoretical analyses; namely, the superscaling properties of cross sections obtained within specific nuclear models have been analyzed with the goals of testing the range of validity of the superscaling hypothesis and of finding and explaining possible scaling violations [9, 10, 11, 12, 13, 14, 15, 16, 17, 18, 19]. Lepton-nucleus scattering in the region of the Δ resonance has been recently studied in [20, 21] and an extension of the scaling formalism to neutral current neutrino processes has also been proposed [22, 23, 24].

The general procedure adopted in scaling analyses consists of dividing the experimental cross sections or separated response functions by an appropriate single-nucleon cross section, containing contributions from protons and neutrons, in order to obtain a reduced cross section which is then plotted as a function of an appropriate variable, itself a function of the energy and momentum transfer. If the result does not depend on the momentum transfer, we say that scaling of the 1st kind occurs. If, additionally, the reduced cross section has no dependence on the nuclear species, one has scaling of the 2nd kind. The simultaneous occurrence of scaling of both kinds is called superscaling.

The superscaling properties of electron-nucleus scattering data in the quasielastic (QE) region have been extensively studied in [3, 4] and in [5]: scaling of the 1st kind was found to be reasonably well respected at excitation energies below the QE peak, whereas scaling of 2nd kind is excellent in the same region. At energies above the QE peak both scaling of the 1st and, to a lesser extent, 2nd kinds were shown to be violated because of the important contributions introduced by effects beyond the impulse approximation: inelastic scattering [5, 6, 25], correlations and meson-exchange currents (MEC) in both the 1p-1h and 2p-2h sectors [18, 19, 26, 27, 28, 29, 30], which mostly reside in the transverse channel.

The variety and complexity of contributions that are present above the QE peak make it difficult to analyze inelastic data directly in terms of inelastic scaling variables and functions. Any analysis of this type requires some kind of theoretical assumption which allows one to

focus on a specific kinematic region, having removed contributions from other processes (to the degree that one can). In [7], the scaling analysis of electron scattering data was extended to the Δ resonance region. A non-quasielastic [1] (non-QE) cross section for the excitation region in which the Δ plays a major role was obtained by subtracting QE-equivalent (see below) cross sections from the data and was found to scale reasonably well up to the peak. Phenomenologically determined QE and non-QE scaling functions were then used to obtain predictions for neutrino cross sections at similar kinematics [7, 8]. This approach has been referred to as the SuperScaling Analysis (SuSA).

In this paper one of our goals is to investigate superscaling, and its violations, in the region above the QE peak, starting from the idea presented in [7]. To this purpose, in Sec. II we begin by reviewing the basic formalism for scaling studies in the QE region; specifically, we summarize the essential features of the so-called SSM-QE model (to be defined in that section). We continue in that section by also considering the Δ region, reviewing and extending the SuSA approach of [7]. All available high-quality data for ^{12}C are reconsidered and analyzed by applying a variety of kinematical cuts to illuminate the origins of the scaling violations that are observed. We then proceed to a deeper investigation of these scaling-violating contributions in the region between the QE and Δ peaks. In order to do so, in Sec. III we present a model for inelastic electron-nucleus scattering within the impulse approximation based on the same superscaling ideas of [7], extending an earlier superscaling-based model for inelastic scattering [6] — this is the so-called SSM-inel approach and has a variant denoted SSM-Δ — see that section for specific definitions. These models are used in Sec. III B to compute non-QE superscaling functions and to compare these with the experimental data and with the SuSA fit for several choices of kinematics. By subtracting theoretical inelastic cross sections from the experimental data, in Sec. IV we then use this model to isolate the non-impulsive components of the cross section and analyze their behavior in terms of 2p-2h MEC contributions obtained in previous studies. Finally, in Sec. V we summarize our study and draw our conclusions, including some remarks of relevance for studies of neutrino reactions with nuclei.

[1] In [7] this residual was called the "Delta" contribution, assuming the Δ to be dominant. To avoid confusion with later discussions where Δ-dominance is assumed, in the present work we denote the entire residual after the quasielastic contribution is removed by "non-QE".

II. FORMALISM AND PREVIOUS RESULTS

A. Scaling in the QE region: the SSM-QE approach

Here we present a summary of the relevant formalism for scaling studies in the QE region, focusing on the formulae and results which will be used in the rest of our study. We denote this the SuperScaling Model for the QE response functions (SSM-QE). Our purpose is to illustrate how scaling ideas can be used to motivate the construction of superscaling-based models for electron-nucleon cross sections, in the spirit of [6, 7] where more extensive discussions can be found.

Within the Relativistic Fermi Gas (RFG) model the only parameter characterizing the nuclear dynamics is the Fermi momentum k_F. In the following we will retain only the lowest orders in an expansion in the parameter $\eta_F = k_F/m_N$, m_N being the mass of the nucleon. Within this approximation the RFG longitudinal (L) and transverse (T) quasielastic response functions, at momentum transfer $\mathbf{q}$ and energy transfer ω, can be written as

$$R^{QE}_{L,T}(\kappa,\lambda) = \frac{1}{k_F} f_{RFG}(\psi) G^{QE}_{L,T}\,, \tag{1}$$

where the scaling function is given by

$$f_{RFG}(\psi) = f^L_{RFG}(\psi) = f^T_{RFG} = \frac{3}{4}(1-\psi^2)\theta(1-\psi^2) \tag{2}$$

and the scaling variable ψ is

$$\psi = \frac{1}{\sqrt{\xi_F}} \frac{\lambda - \tau}{\sqrt{(1+\lambda)\,\tau + \kappa\sqrt{\tau\,(1+\tau)}}}\,, \tag{3}$$

with $\xi_F \equiv \sqrt{1+\eta_F^2} - 1$. In the formulae above we have introduced the usual dimensionless variables: $\kappa \equiv q/2m_N$, $\lambda \equiv \omega/2m_N$ and $\tau \equiv \kappa^2 - \lambda^2$. Retaining terms only up to order η_F, the functions $G^{QE}_{L,T}$ are given by [5]

$$G^{QE}_L = \frac{\kappa}{2\tau}\left\{Z\left[(1+\tau)W^{QE}_{2,p} - W^{QE}_{1,p}\right] + N\left[(1+\tau)W^{QE}_{2,n} - W^{QE}_{1,n}\right]\right\} \tag{4}$$

$$G^{QE}_T = \frac{1}{\kappa}\left\{ZW^{QE}_{1,p} + NW^{QE}_{1,n}\right\}\,, \tag{5}$$

$W^{QE}_{(1,2),p(n)}$ being the single-proton (-neutron) electromagnetic structure functions, which are given in terms of electromagnetic form factors by

$$W^{QE}_{1,p(n)} = \tau G^2_{M,p(n)}(\tau) \tag{6}$$

$$W^{QE}_{2,p(n)} = \frac{1}{1+\tau}\left[G^2_{E,p(n)}(\tau) + \tau G^2_{M,p(n)}(\tau)\right]\,. \tag{7}$$

Given the response functions, the QE cross section is then obtained as

$$\frac{d\sigma}{d\epsilon' d\Omega} = \sigma_M \left[v_L R_L^{QE} + v_T R_T^{QE} \right] , \tag{8}$$

where ϵ' is the outgoing electron energy and $\Omega = (\theta, \phi)$ is the solid angle for the scattering. Here σ_M is the Mott cross section and $v_{L,T}$ are the usual kinematic factors.

The expressions above suggested, instead of using the RFG scaling function in Eq. (2) that one may work backwards to obtain an experimental scaling function by dividing the QE cross sections by the quantity

$$S^{QE} = \sigma_M \left[v_L G_L^{QE} + v_T G_T^{QE} \right] \tag{9}$$

and then, for use in discussions of 2nd-kind scaling, multiplying the result by k_F:

$$f^{QE}(\psi, \kappa) = k_F \frac{(d\sigma/d\epsilon' d\Omega)^{exp}}{S^{QE}} . \tag{10}$$

Separate L and T scaling functions can similarly be obtained as

$$f_{L,T}^{QE}(\psi, \kappa) = k_F \frac{R_{L,T}^{exp}}{G_{L,T}^{QE}} . \tag{11}$$

In our previous analyses of the world (e, e') data we have found that, for large enough momentum transfer ($q > 2k_F$), 1st-kind scaling works rather well for values of energy transfer ω below the QE peak value, ω_{QE}. For large values of ω deviations are observed, coming from contributions beyond QE scattering, such as inelastic scattering and MEC effects. A separate analysis of the longitudinal and transverse channels shows that these deviations mainly occur in the transverse response, while the experimental longitudinal reduced cross sections scale much better and up to larger values of ω. This suggests that we can use the longitudinal QE experimental scaling function obtained in [3, 4] to define a phenomenological scaling function.

In particular, assuming that (i) indeed there is a universal superscaling function and that (ii) it can be identified with the phenomenological function extracted from the analysis of the QE longitudinal response, we can now work backwards and use this superscaling hypothesis to predict cross sections. To be more specific, we define the superscaling model for the QE response functions (*i.e.,* what we are calling the SSM-QE approach in this work). This consists in using Eq. (1), but with

$$f^{SSM-QE}(\psi) \equiv f_L^{QE}(\psi) . \tag{12}$$

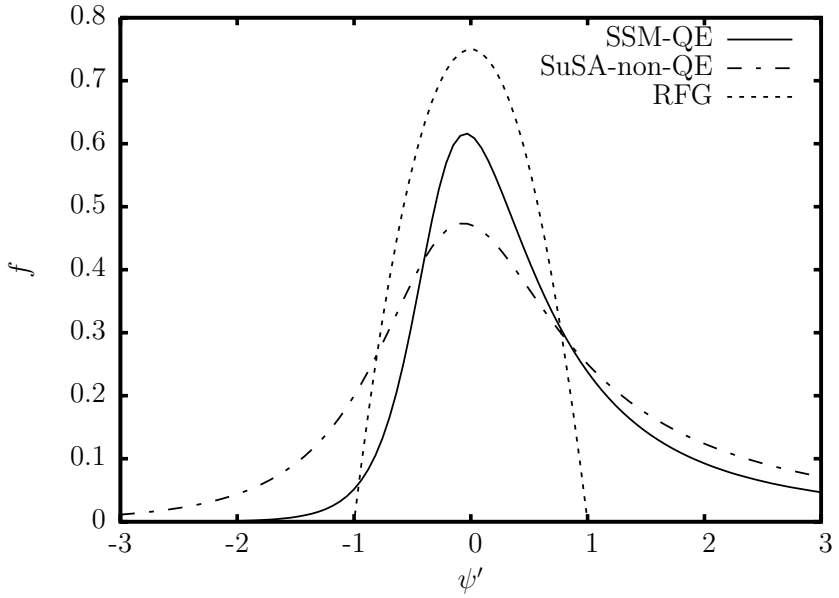

FIG. 1: Phenomenological fits for the superscaling functions f^{SSM-QE} (solid line) and f^{non-QE}_{SuSA} (dot-dashed) versus the appropriate scaling variable. The RFG superscaling function is also shown for comparison (dotted line).

An important step has been taken here: only the longitudinal cross sections are employed in defining the phenomenological scaling function. This choice is based on the fact that the transverse cross sections can have significant non-QE or non-impulsive contributions, for instance, the former from inelastic excitations of the nucleon (importantly the Δ) and the latter from 2p-2h MEC — see the discussions to follow in the present work. However, in lowest order these are not very important in the longitudinal cross section, and thus it provides the only opportunity to isolate the impulsive contributions to the nuclear response.

The phenomenological function f^{SSM-QE} employed in the present approach is shown in Fig. 1 (solid line), where it is compared with the RFG scaling function of Eq. (2) (dotted line). Also shown is the phenomenological non-QE scaling function, f^{non-QE}_{SuSA} to be defined below in the following subsection (dot-dashed line). Focusing on the phenomenological QE scaling function, one sees that it is significantly different from the RFG result: it is about 17% lower at the peak and is asymmetric, having a tail that extends to higher ω (in the positive ψ' direction). In fact, subsequent to obtaining the phenomenological results shown in the figure [3, 4], relativistic mean field theory (RMF) was employed to obtain theoretical scaling functions. This approach is especially relevant at high energies where relativistic effects are known to be important. These RMF studies yielded essentially the same longitudinal

scaling function as the phenomenological model [11], and the required asymmetric shape of the scaling function was obtained theoretically. We shall return below to comment on the RMF transverse scaling function. Still later a so-called semi-relativistic approach was pursued [12], again yielding essentially the same results. More recently, a deceptively simple "BCS-inspired" model was developed [31], with the same outcome: a peak height that is significantly below the RFG result and an asymmetric shape. Within the flexibility in each model and the experimental uncertainties one can say that a single longitudinal QE scaling function has clearly emerged.

In passing, we note that, as is usually done in studies of electron scattering in order to reproduce the correct position of the QE peak, in the present study we have introduced a small energy shift E_{shift}. Within the framework of the superscaling formalism outlined above, this amounts to considering a "shifted" scaling variable ψ', calculated according to Eq. (3), but with $\lambda \rightarrow \lambda' = \lambda - E_{shift}/2m_N$ and $\tau \rightarrow \tau' = \kappa^2 - \lambda'^2$. The values $k_F = 228$ MeV/c and $E_{shift} = 20$ MeV have been used in all of the calculations for ^{12}C presented here and in the following sections.

Having found that the longitudinal QE scaling function is universal, whether treated phenomenologically or via models for 1p-1h knockout reactions, we now discuss the transverse QE response. In most approaches one finds that once the single-nucleon cross section is removed in defining scaling functions as above the longitudinal and transverse answers are basically the same, *i.e.,* one has what has been called scaling of the 0th kind with $f_T(\psi') = f_L(\psi')$. However, in what is likely the best model employed so far, the RMF approach cited above, one finds that 0th-kind scaling is mildly broken for momentum transfers in the 1 GeV region with $f_T(\psi') > f_L(\psi')$. For instance, at $q = 500$ MeV/c (1000 MeV/c) the transverse RMF scaling function is 13% (20%) larger at its peak than is the longitudinal one. On the other hand, from analyses of 1p-1h MEC contributions [26, 27, 28, 29, 30] one sees the opposite behavior, namely, the 1-body (impulse approximation) and 2-body MEC contributions to the 1p-1h response, which must occur coherently and hence can interfere, in fact do so destructively and therefore a somewhat lower result is found for the total transverse scaling function. Neither of these effects is seen in the longitudinal response in leading order. Unfortunately, no single model exists where one has adequate relativistic content (as in the case of the RMF approach) and has a consistent way to obtain the MEC contributions; indeed, the MEC studies cited above could not be attempted on the same

footing as the 1-body RMF computations and could only be undertaken using much simpler dynamics.

Accordingly, we have no better option at present than to adopt some working procedure. Henceforth we shall assume that 0th-kind scaling is obeyed and thus take $f_T(\psi') = f_L(\psi')$ for the quasielastic response. One should remember, however, that this may not be completely true and that the QE transverse response could be either a bit larger or a bit smaller than the one obtained under this assumption. In Sec. IV, where the scaling-based cross sections are compared with data, we shall return to discuss these issues in somewhat more detail.

B. The SuSA approach to scaling in the Δ region

We begin by summarizing the essentials of the SuSA approach taken in [7], where non-QE cross sections were obtained from experimental inclusive inelastic electron-nucleus cross sections by subtracting QE cross sections given by the SSM-QE procedure described above. Namely the following cross sections

$$\left(\frac{d\sigma}{d\epsilon' d\Omega}\right)^{non-QE} \equiv \left(\frac{d\sigma}{d\epsilon' d\Omega}\right)^{exp} - \left(\frac{d\sigma}{d\epsilon' d\Omega}\right)^{SSM-QE} \tag{13}$$

were obtained as a first step. In the earlier work it was assumed that Δ-dominance could be invoked. Namely, in analogy with the QE results of previous section, a model in which only impulsive contributions proceeding via excitation of an on-shell Δ was employed. In that model the leading-order RFG expressions for the electromagnetic response function can be written as [7, 32]:

$$R^{\Delta}_{L,T}(\kappa,\lambda) = \frac{1}{k_F} f^{\Delta}(\psi_{\Delta}) G^{\Delta}_{L,T} \tag{14}$$

with $f^{\Delta}(\psi_{\Delta}) = f_{RFG}(\psi_{\Delta})$ and

$$\psi_{\Delta} = \frac{1}{\sqrt{\xi_F}} \frac{\lambda - \tau\rho_{\Delta}}{\sqrt{(1+\lambda\rho_{\Delta})\,\tau + \kappa\sqrt{\tau\,(1+\tau\rho_{\Delta}^2)}}}\,, \tag{15}$$

with

$$\rho_{\Delta} = 1 + \frac{\mu_{\Delta}^2 - 4\tau}{4\tau}\ ;\ \mu_{\Delta} = \frac{m_{\Delta}}{m_N} \tag{16}$$

and with

$$G^{\Delta}_{L} = \frac{\kappa}{4\tau} A \left[\left(1+\tau\rho_{\Delta}^2+1\right) w_2^{\Delta} - w_1^{\Delta}\right] \tag{17}$$

$$G^{\Delta}_{T} = \frac{1}{2\kappa} A w_1^{\Delta}\,. \tag{18}$$

In Eqs. (17,18) the single-hadron $N \to \Delta$ structure functions are [2]

$$w_1^\Delta = \frac{1}{2}\left(\mu_\Delta + 1\right)^2 \left(2\tau\rho_\Delta + 1 - \mu_\Delta\right)\left(G_{M,p}^2 + 3G_{E,n}^2\right) \tag{19}$$

$$w_2^\Delta = \left(\mu_\Delta + 1\right)^2 \frac{\left(2\tau\rho_\Delta + 1 - \mu_\Delta\right)}{1 + \tau\rho_\Delta}\left(G_{M,p}^2 + 3G_{E,n}^2 + 4\frac{\tau}{\mu_\Delta^2}G_{C,\Delta}^2\right), \tag{20}$$

where the magnetic, electric and Coulomb form factors are taken to be

$$G_{M,p} = 2.97 g_\Delta(\tau) \tag{21}$$

$$G_{E,n} = -0.03 g_\Delta(\tau) \tag{22}$$

$$G_{C,\Delta} = -0.15 G_{M,p}(\tau), \tag{23}$$

with

$$g_\Delta(\tau) = \frac{1}{\sqrt{1+\tau}}\frac{1}{\left(1 + 4.97\tau\right)^2}. \tag{24}$$

Starting from these expressions and assuming that the only non-QE contributions arise from this Δ-dominance model one can define a superscaling function in the region of the Δ peak as follows

$$f^{non-QE}(\psi_\Delta) \equiv k_F \frac{\left(\frac{d\sigma}{d\epsilon' d\Omega}\right)^{non-QE}}{S^\Delta} \tag{25}$$

with

$$S^\Delta \equiv \sigma_M \left[v_L G_L^\Delta + v_T G_T^\Delta\right]. \tag{26}$$

We have performed an analysis similar to that presented in [7] and, focusing on scaling of the 1st kind, we have considered all available high-quality data of inelastic electron scattering cross sections on ^{12}C [33, 34, 35, 36, 37, 38, 39, 40, 41, 42]. The functions f^{non-QE} we obtain are shown in Fig. 2. Note that, as above, we have introduced a small energy shift E_{shift}. In employing Eqs. (15) and (16) we do as in the QE case and replace λ by λ', and τ by τ'. As before, for ^{12}C the values $k_F = 228$ MeV/c and $E_{shift} = 20$ MeV have been used in all of the calculations presented here and below.

Overall we see a tendency for coalescence below and up to the Δ peak for some, but not all, of the data. Specifically, for kinematics lying below the Δ peak ($\psi'_\Delta = 0$) these

[2] Equations (19,20) should be taken with $A = Z$ and the $p \to \Delta^+$ structure functions and with $A = N$ and the $n \to \Delta^0$ structure functions, and then summed, but since these processes are purely isovector we use $A = N + Z$ with one choice for the structure functions.

non-QE results scale reasonably well given the assumption of Δ-dominance, showing scaling violations at the level of roughly 0.1 units of scaling function, versus the QE peak value of about 0.6, namely scaling violations of approximately 15–20%. As discussed in more detail later, since we cannot have any inelasticity over much of this kinematic range (being below pion production threshold) one must suspect that effects such as from 2p-2h MEC contributions are playing a non-trivial role. Nevertheless, accepting this as a measure of the potential uncertainty in following the straightforward SuSA approach, in [7] an empirical fit to these results, f_{SuSA}^{non-QE}, was obtained and then used to predict neutrino-nucleus cross sections in the Δ region. It should be stressed that the assumption of Δ-dominance is clearly only an approximation; in the following sections we present a more microscopic approach in which the superscaling approach discussed above for the QE region is extended to the inelastic region (denoted the SSM-inel approach; see Sec. III) and where non-impulsive 2p-2h MEC effects are considered separately (see Sec. IV).

Looking in more detail, let us first consider the two bottom panels of Fig. 2, which show all available high-quality data for ^{12}C and the data with momentum transfers $q > 500$ MeV/c. We observe that many (but not all) of the data indeed tend to collapse into a single function close to the Δ peak. The spreading of the data is larger than what was observed in similar analyses of QE data, but a tendency to cluster (scale) is seen, at least for a subset of the data. In order to discuss scaling, and the breaking of it, one may consider three different regions. First, in the positive ψ'_Δ region the spreading of the data increases and the data themselves tend to diverge. This behavior is analogous to what happens for the QE case for large values of ψ' and it is due to the presence of contributions coming from higher resonances. Second, for $\psi'_\Delta < -1$ the data form a relatively uniform background showing no specific pattern. This is the range where effects from 2p-2h MEC are expected to play a significant role (see below). Finally there is the region $-1 < \psi'_\Delta < 0$, where the spreading of the data is somehow less evident and where both type of scale-breaking effects can contribute.

In a first attempt to disentangle these effects, in the top right-hand and two middle panels of the figure we apply a progression of cuts on the data, specifically taking those with 0.5 GeV/c $< q < q_{cut}$, where q_{cut} goes from 1 to 2 GeV/c. As the cut tightens we expect to have fewer and fewer contributions from higher inelasticities. For completeness, and for a better understanding of the whole figure, in the upper left-hand panel we also report the data for

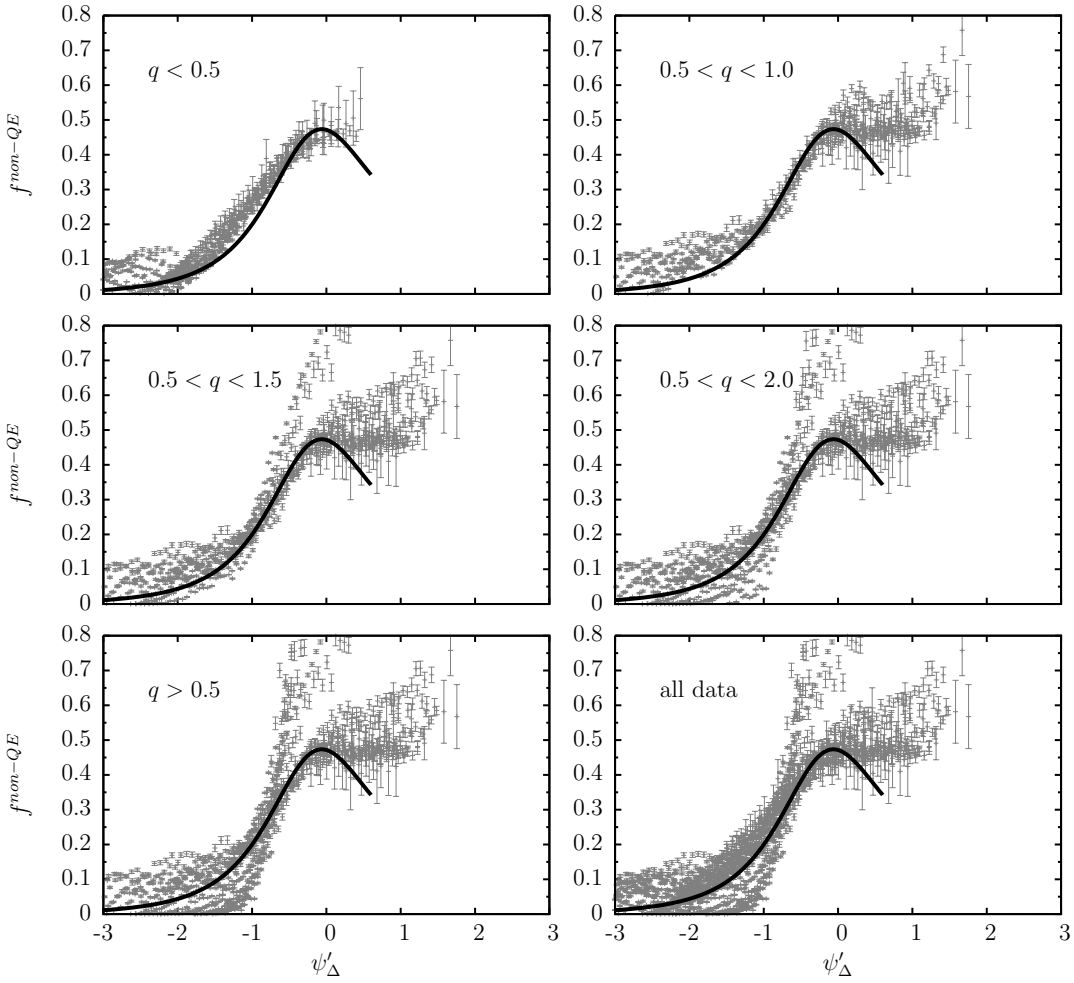

FIG. 2: "Experimental" superscaling function f^{non-QE} for ^{12}C, obtained by applying the QE-subtraction procedure described in the text to the available experimental data for ^{12}C. The function is plotted versus the Δ scaling variable ψ'_Δ. Kinematical cuts on the values of the momentum transfer q (in GeV/c) are considered, as indicated in each panel. A phenomenological fit of the non-QE superscaling function, f^{non-QE}_{SuSA}, is also shown for comparison by the solid line.

low momentum transfer ($q < 0.5$ GeV/c).

The results shown in the different panels seem to indicate that the presence of contributions from higher inelasticities corresponds to values of f^{non-QE} which lie above the average scaling function for $-0.5 < \psi'_\Delta < 0$ and below it for $-1 < \psi'_\Delta < -0.5$ (for instance, compare the top and middle right-hand panels). In particular we observe data sets which seem to cross the average function around $\psi'_\Delta = -0.6$. They correspond to JLab cross section data taken at an incident energy of 4.045 GeV and scattering angles between 23 and 74 degrees, for which there is indeed a strong overlap of the Δ and higher inelastic contributions.

The observations above suggest that, if we are interested in obtaining a phenomenological

SuSA scaling function for the Δ region alone, f_{SuSA}^{non-QE}, these highly inelastic data sets should be excluded from the fit. Such a fit, similar to that obtained in [7], is indicated in Fig. 2 by the solid line, and in Fig. 1 it is compared with the phenomenological fit for the QE region and, for reference, with the RFG scaling function.

We observe that f_{SuSA}^{non-QE} differs significantly from f^{SSM-QE}. This is expected, because, besides incorporating initial-state dynamics, the phenomenological non-QE scaling functions certainly contain additional effects, such as those due to the finite width of the Δ resonance, as well as potential 2p-2h MEC contributions. However it is interesting to investigate whether or not these differences can be explained only in terms of kinematics and of trivial effects, such as the finite width of the Δ, or whether also differences in the nuclear dynamics at the QE and Δ peaks can contribute to them. In order to address this issue we need to introduce some model for the cross sections in the Δ region, and we will present this in the next section.

Let us conclude this section by introducing the phenomenological SuSA model for the Δ region [7] mentioned in the introduction. Following the approach used in previous section for the QE case, we can obtain the response functions for Δ excitation from Eqs. (14), by substituting the RFG expression for f^{Δ} with the phenomenological fit obtained from the data, namely

$$R_{L,T}^{SuSA-\Delta,}(\kappa,\lambda) = \frac{1}{k_F} f_{SuSA}^{non-QE}(\psi_{\Delta}) G_{L,T}^{\Delta}\,. \tag{27}$$

This model was tested in [7] for electron scattering over a range of kinematics, showing agreement with the data at the level of 10% or better.

III. SSM-BASED MODELS FOR THE INELASTIC REGION

In this section we develop a model for the response functions in the inelastic region lying above the QE peak, basing the approach on the assumption of universality of the superscaling function, *i.e.,* using the same SSM approach employed for the QE region. This will allow us to address two issues. On the one hand we will explore the origin of the difference between the phenomenological scaling functions obtained by fitting the data for the QE (f^{SSM-QE}) and Δ (f_{SuSA}^{non-QE}) regions, as discussed in the last section. We will start by assuming that this difference can be accounted for only by kinematics and finite width effects, and we will compare the scaling function obtained under this hypothesis with the experimental one.

On the other hand, we will investigate further the role played by contributions from higher resonances in producing the scaling violations shown by the experimental f^{non-QE} in the region $-1 < \psi'_\Delta < 0$.

As the model we present here is based on the impulse approximation, it will not allow us to investigate MEC effects in the $\psi'_\Delta < -1$ region directly, but it will turn out to be useful later in Sec. IV, in presenting the experimental data in a different and more focused way.

A. Formalism

We follow closely the approach of [6], where a microscopic model based on the RFG and on superscaling was used to study highly-inelastic electron-nucleus scattering. The RFG expressions for the inelastic nuclear response functions can be written as [6]:

$$R^{inel}_{L,T} = \frac{1}{k_F}\int_{\mu_1}^{\mu_2} d\mu_X \mu_X f_{RFG}(\psi_X) G^{inel}_{L,T} \,, \tag{28}$$

where ψ_X is obtained from Eqs. (15) and (16) for a generic invariant mass W_X of the final state reached by the nucleon, namely by replacing μ_Δ with $\mu_X = W_X/m_N$. The quantities $G^{inel}_{L,T}$, neglecting terms of order η_F^2 and higher as before, are given by

$$G^{inel}_L = m_N \frac{\kappa}{2\tau}\left\{Z\left[(1+\tau\rho_X^2)\tilde{w}_2^p - \tilde{w}_1^p\right] + N\left[(1+\tau\rho_X^2)\tilde{w}_2^n - \tilde{w}_1^n\right]\right\} \tag{29}$$

$$G^{inel}_T = m_N \frac{1}{\kappa}\left\{Z\tilde{w}_1^p + N\tilde{w}_1^n\right\} \,, \tag{30}$$

where $\tilde{w}_{1,2}$ are the inelastic single-nucleon structure functions, which depend on two variables, the four-momentum transfer Q^2 and the invariant mass W_X or, equivalently the single-nucleon Bjorken variable $x = |Q^2|/[W_X^2 - m_N^2 - Q^2]$ (see also [6]). Note that the inelastic structure functions have dimension of E^{-1}, at variance with the previous QE and Δ cases: for this reason we indicate them as $\tilde{w}$. The integration limits in Eq. (28) are given by

$$\begin{aligned} \mu_1 &= 1 + \mu_\pi \\ \mu_2 &= 1 + 2\lambda - \epsilon_S \end{aligned} \tag{31}$$

with $\mu_\pi = m_\pi/m_N$ and where $\epsilon_S = E_S/m_N$ is the dimensionless version of the nucleon separation energy. The first limit is simply the threshold for pion production, while the second was derived in [6].

Following a procedure analogous to that illustrated for QE scattering, we can now generalize the RFG by making the substitution

$$f_{RFG}(\psi_X) \to f^{SSM-QE}(\psi_X) \equiv f^{SSM-non-QE}(\psi_X) \equiv f^{SSM}(\psi_X) \tag{32}$$

in Eq. (28). This modeling, which we will call SSM-inel in the following, is thus based on the assumption, suggested by the RFG, that there exists only *a single universal scaling function* and that the latter can be identified with the phenomenological fit obtained from the QE longitudinal data. Henceforth, for simplicity we denote the phenomenological (super-) universal scaling function to be used both for impulsive QE and inelastic contributions by f^{SSM}.

Important ingredients of the model are, of course, the single-nucleon structure functions. In our past work [6], which was focused on the highly-inelastic scattering region, we used the Bodek *et al.* [43] parametrizations of the proton and neutron structure functions which were available at the time. However, in recent years new studies, both theoretical [44, 45] and experimental [46, 47, 48, 49], of the nucleon structure functions in the resonance region have been performed, indicating the need for more sophisticated parametrizations. As we are now studying this region, we have updated our calculations using more modern expressions for $\tilde{w}_{1,2}^{p,n}$. We thus use parametrizations recently obtained by Bosted and Christy [50], both for the proton [46] and neutron [47] structure functions. We note that all details regarding the nucleon resonances, such as finite widths, are automatically included in the parametrization and that we do not consider any possible medium-modification of single-hadron properties.

In order to understand better the role played by higher resonances, we also consider a variant of the full SSM-inel model. For this approach, denoted SSM-Δ, we consider contributions coming only from $N \to \Delta$ excitations, which we describe in terms of form factors, and we take the finite width of the Δ explicitly into account. Following [32] we start with

$$R_{L,T}^{\Delta} = \int_{\mu_1}^{\mu_2} \frac{1}{\pi} \frac{\Gamma(\mu_X)/2m_N}{(\mu_X - \mu_\Delta)^2 + \Gamma(\mu_X)^2/4m_N^2} R_{L,T}^{\Delta}(\kappa, \lambda, \mu_X) d\mu_X \,, \tag{33}$$

where $R_{L,T}^{\Delta}(\kappa, \lambda, \mu_X)$ are the RFG response functions of Eq. (14) calculated using a generic nucleon excitation invariant mass μ_X, and ψ_X is obtained from Eq. (15) for $\mu_\Delta \to \mu_X$. Once again we then generalize the RFG model by substituting for the RFG scaling function in Eq. (14) the universal one, $f^{\Delta}(\psi_X) \to f^{SSM}(\psi_X)$. The integration limits in Eq. (33) are those of Eqs. (31), and the μ_X dependence of the Δ width Γ is given by

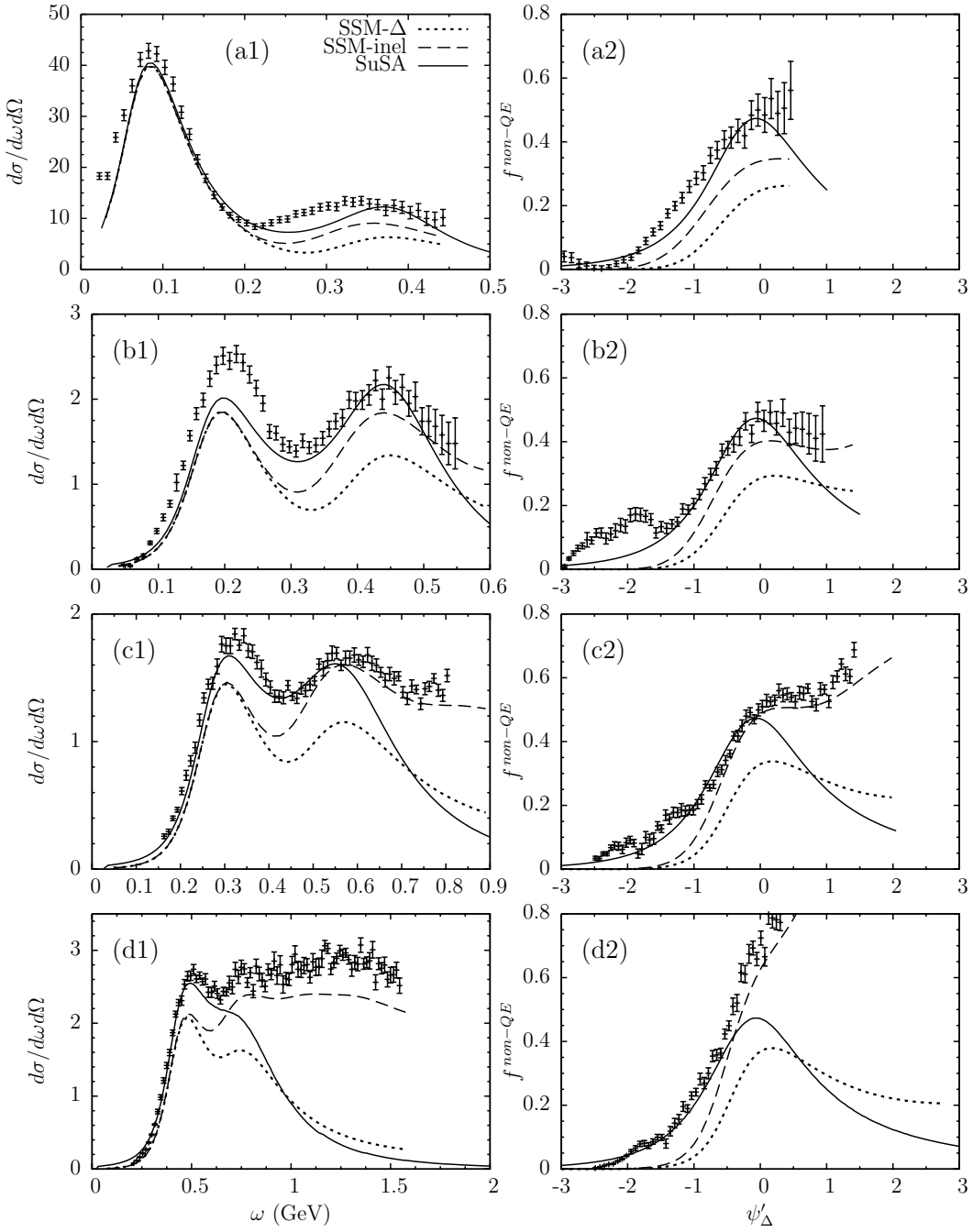

FIG. 3: Cross sections in nb/sr/MeV (left-hand panels; SSM-QE results also included) and non-QE superscaling functions (right-hand panels) for ^{12}C, calculated within the SSM-inel (dashed line) and SSM-Δ (dotted) approaches, and compared with the phenomenological SuSA results (full line). The kinematics selected here are summarized in Table I; the data are taken from from [34, 35, 36].

$$\Gamma(\mu_X) = \Gamma_0 \frac{\mu_\Delta}{\mu_X} \left(\frac{p_\pi^\star}{p_\pi^{res}} \right)^3 \tag{34}$$

with $\Gamma_0 = 120$ MeV,

$$p_\pi^\star = \frac{m_N}{\mu_X} \left[\frac{(\mu_X^2 - 1 - \mu_\pi^2)^2}{4} - \mu_\pi^2 \right]^{\frac{1}{2}} \tag{35}$$

and where p_π^{res} is obtained from Eq. (35) with $\mu_X = \mu_\Delta$. We then compute inclusive cross sections using the response function in Eq. (33) and, in order to obtain superscaling functions within this model, namely $f^{SSM-\Delta}(\psi_\Delta)$, as usual we divide the cross sections by S^Δ/k_F, where S^Δ is the factor given in Eq. (26). These superscaling functions may then be compared with the phenomenological SuSA one, $f_{SuSA}^{SSM-inel}(\psi_\Delta)$, discussed above [Eq. (25)].

B. Results

In this section we illustrate the results for the superscaling function obtained using the SSM-inel and SSM-Δ models, together with the phenomenological SuSA fit. Before studying the behavior of the non-QE scaling function over the whole range of kinematics considered in Fig. 2, we will present a few selected examples of cross sections and scaling functions. The use of cross sections allows a direct comparison with "real" and more familiar data, and the selection of fixed kinematics can illustrate better the characteristics, and the limits, of the models. This comparison is shown in Fig. 3, where the left-hand panels show results for cross sections and the right-hand panels show results for non-QE scaling functions. For illustration, we choose to consider kinematics covering a limited range of energy and momentum transfer, large enough so that the Δ excitation is clearly present and small enough so that higher inelastic contributions do not overlap completely with the QE and Δ peaks. Specifically, we select a lower limit case (panels a1, a2) corresponding to incident energy $\epsilon = 620$ MeV and scattering angle $\theta = 36°$, and an upper limit case (panels d1, d2) with $\epsilon = 3595$ MeV and $\theta = 16°$. In order to explore the angle dependence of the cross sections and scaling functions, in the middle panels we show results for intermediate kinematics with two choices of scattering angle, $\epsilon = 680$ MeV, $\theta = 60°$ (panels b1,b2) and $\epsilon = 1299$ MeV, $\theta = 37.5°$ (panels c1,c2). The kinematics are summarized in Table I which contains as well the momentum transfers at the QE and Δ peaks, q_{QE} and q_Δ, respectively.

In the figure we compare the results obtained using our SSM-inel and SSM-Δ models with

Case	ϵ [MeV]	θ [deg]	q_{QE} [MeV/c]	q_{Δ} [MeV/c]
a	620	36	366	460
b	680	60	606	600
c	1299	37.5	791	850
d	3595	16.02	1056	1189

TABLE I: ^{12}C(e,e') kinematics considered

those corresponding to the SuSA fit introduced at the end of Sec. II B. The SSM-Δ model is certainly an overly simple one and, as can be seen from Fig. 3, the corresponding curves show the largest discrepancies with the data. However, the SSM-Δ results are qualitatively interesting because, when compared with the SSM-inel results, they allow us to some extent to disentangle the effects related to contributions arising from higher resonances, which cannot be eliminated from the data.

The cross sections plotted in the left-hand column of the figure include the QE contribution calculated within the SSM-QE modeling outlined in Sec. II A, which is the same for all models. Differences between the various curves in the QE region are therefore due to differences in the non-QE part of the cross sections obtained using the various models. By looking at the cross sections we can clearly see that our inelastic model always underestimates the data in both QE and, especially, inelastic regions. More specifically, for small incident energy (upper panels) the QE peak is well reproduced. At the Δ peak both SSM models clearly underestimate the data, while SuSA obviously reproduces the peak reasonably, since it was fit to the data. All models are unable to reproduce the cross section completely in the region between the QE and Δ peaks.

Similar results hold for the Δ-peak region at larger scattering angles (panel b1). We notice that in this case the SSM and SuSA modeling underestimates the data even at the QE peak. This is related to the fact that at large scattering angles the transverse contribution is dominant. Previous scaling studies [3, 4] in fact showed that the transverse QE superscaling function extracted from the data differs from the longitudinal one and exhibits stronger scaling violations. We attribute these differences to contributions beyond the impulse approximation, such as 2p-2h MEC and correlations, which are not included in the models discussed in this section (see, however, Sec. IV). Moreover, at larger angles the

overlap between the QE and Δ peaks becomes more significant, which explains the difference between SuSA and SSM models at the QE peak.

The same considerations can be extended to the case of higher incident energies (panels c1 and d1). We observe that in these cases the SSM-Δ results decrease very rapidly at large energy transfer, as does the SuSA curve, because no higher inelastic contributions beyond the Δ are included. The SSM-inel curve has an ω-dependence similar to that of the data for large energy transfer, suggesting that the single-nucleon inelastic content has been correctly implemented in the model. However, the experimental cross sections are again underestimated even in the higher inelastic region.

With these considerations about cross sections in mind, we can now examine the right-hand panels of the figure, which show the non-QE scaling functions. We can summarize our findings as follows. As already said, the SSM-inel model always underestimates the data. This difference, in both size and shape, is particularly relevant for small incident energies and, at all kinematics, for relatively large negative values of the scaling variable ψ'_Δ. At very low energy (upper panels of the figure) or for $\psi'_\Delta < -1$ this is expected, because in these regions effects stemming from correlations and 2p-2h MEC can play an important role [18, 19] and they cannot be reproduced by models which assume impulsive, quasi-free scattering on bound nucleons.

In the region $-1 < \psi'_\Delta < 0$ the theoretical SSM-inel curves still fall below the data, but their shape is similar to that displayed by the experimental scaling function. The discrepancies are larger below $\psi'_\Delta = -0.5$, where 2p-2h MEC may still contribute sizably, whereas when approaching the Δ peak the theoretical curves lie closer to the data. The conclusion we draw from these observations is that the basic idea of the phenomenological superscaling-based model (SSM-inel) is probably correct and that it can account for most of the difference in shape between the experimental QE and non-QE scaling functions, but that the model presented here is still too simple and needs some improvements in order to be considered quantitatively reliable. In particular, as previously observed, the model assumes universality of the longitudinal and transverse QE scaling function, *i.e.,* the so-called scaling of the 0th kind, which has been shown to be violated by the QE data. While part of this violation can be ascribed to correlation and 2p-2h MEC effects, as discussed in the next section, a certain amount of it could be present even at the impulse approximation level, and, if so, should be incorporated in the model by using different scaling functions for the

T and L responses. This would lead to a renormalization of the calculated cross sections and non-QE scaling functions, which may fill some of the discrepancy with the data at the Δ peak. Unfortunately, such an improvement of the model is not straightforward, although work is now in progress along this line.

If we accept that at least some of the difference in normalization between the data and the calculated f^{non-QE} close to the Δ peak can be accounted for by an improvement in the scaling functions used as ingredients in the model, then the SSM-inel results obtained so far can provide some useful additional insight on the behavior of the Δ superscaling function. In Fig. 4 we plot the function f^{non-QE} for a relatively large set of kinematics (indicated in the key inside the figure) corresponding approximately to values of the momentum transfer in the range 500-1500 MeV/c. The top panel shows the experimental non-QE scaling functions, the middle panel those obtained within the SSM-inel model and the bottom panel those calculated with the SSM-Δ model. We see that both the data and the SSM-inel scaling functions present the same type and degree of scaling violations in the region $-1 < \psi'_\Delta < 0$, with the curves corresponding to the highest momentum transfer being the lowest ones for approximately $\psi_\Delta < -0.5$ and then becoming the highest one for larger values of the scaling variable. In contrast, this behavior is practically absent in the SSM-Δ results, suggesting that scaling violations in the region $-1 < \psi'_\Delta < 0$ are essentially due to contributions from higher resonances. This observation has important consequences for SuSA modeling of neutrino cross sections [7], because it supports the validity of using the universal scaling function f^{SSM} in predicting cross sections for kinematical conditions in which only contributions up to the excitation of the Δ resonance are relevant.

Still looking at Fig. 4, let us mention that both SSM models provide scaling-violations at the Δ peak which seem to be larger than those exhibited by the data. In our study we have checked that this is due to kinematical effects, being related to the interplay between integration limits and the dependence of the variable ψ'_X upon the invariant mass μ_X. The inclusion of some degree of scaling-violation in the phenomenological scaling function used in the model may solve this problem.

The differences in the behavior of the theoretical and experimental scaling functions at the peak of the Δ may also be related to the different role of final-state interactions (FSI) for QE scattering and Δ excitation. In fact, previous studies in the QE region have shown that the phenomenological QE scaling function is affected by FSI at the right of the QE peak

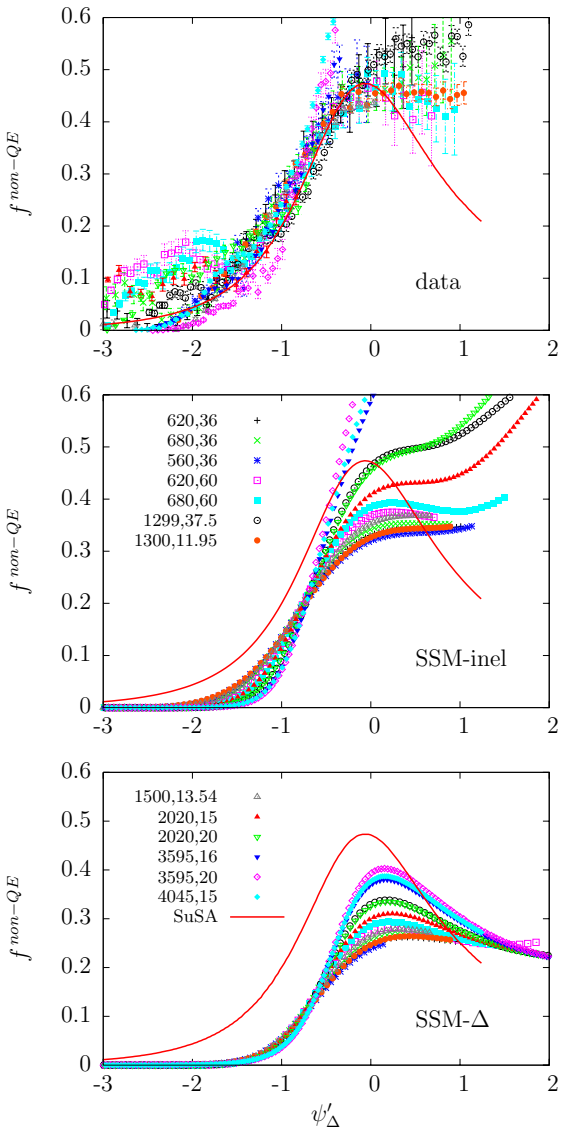

FIG. 4: (Color online) Experimental "QE subtracted" data for f^{non-QE} for ^{12}C for a variety of kinematics (top panel) and corresponding results of the SSM-inel model (middle) and of the SSM-Δ model (bottom). The kinematics considered are labeled with ϵ (MeV) and θ (deg). The SuSA fit is shown by the solid (red) line. The values of the momentum transfer for the kinematics presented here fall approximately in the interval $0.5 < q < 1.5$ GeV/c.

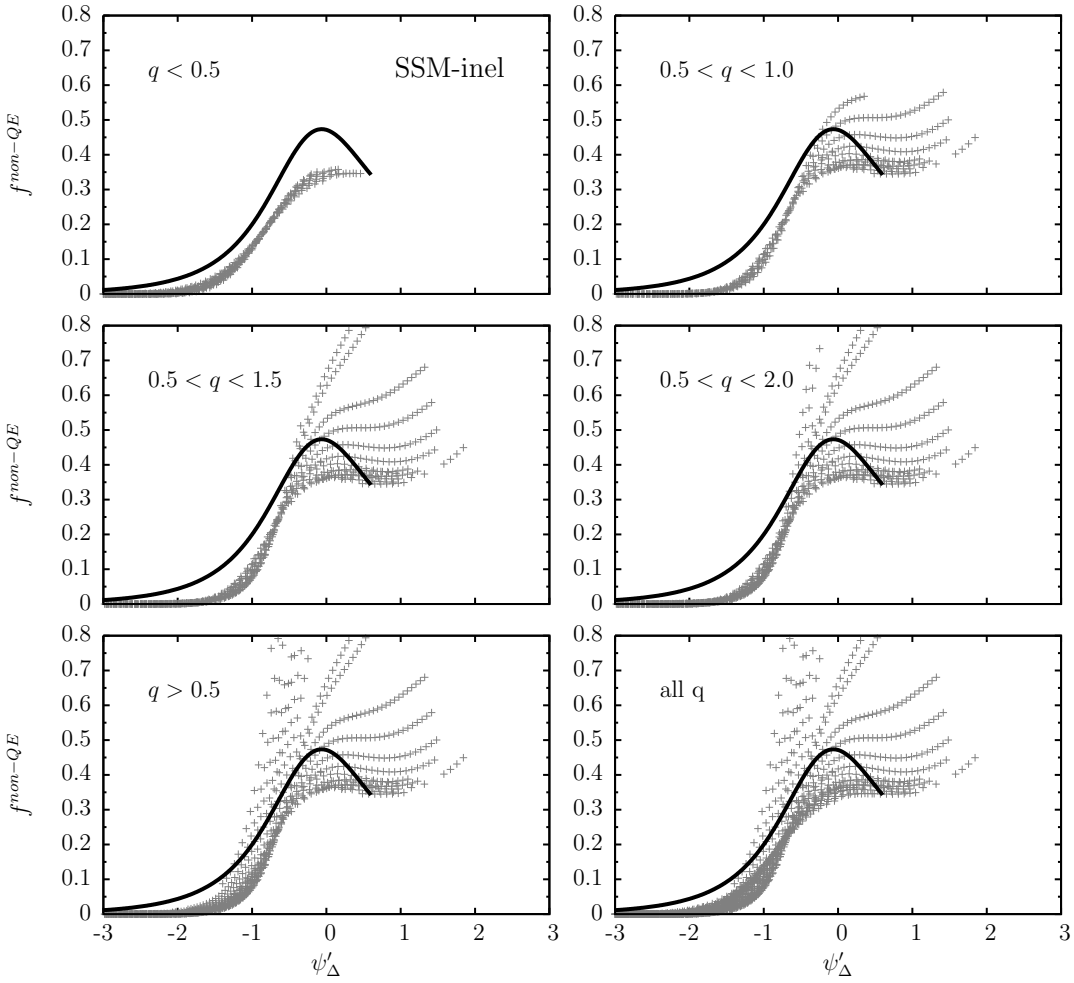

FIG. 5: Non-QE superscaling function for ^{12}C calculated within the SSM-inel model versus the Δ scaling variable ψ'_Δ. The same kinematical cuts as in Fig. 2 are considered, as indicated in the different panels. The phenomenological fit of the non-QE superscaling function is also shown for comparison (solid line).

where FSI produce a tail, and partially at the peak, since a larger tail at positive ψ results in a smaller maximum value of the scaling function. While the tail of the phenomenological function contributes very little to the calculated non-QE scaling function at the left of the Δ peak due to the limits of integration (see Eqs. (28, 31 and 33)), its maximum value may have some relevance at the Δ peak. Some details concerning the limits of integration and the role of f^{SSM} in determining the non-QE scaling function can be found in the Appendix.

Finally, before proceeding in the next section to the analysis of the residual after impulsive contributions have been removed, and to complete the overview of our results for the function f^{non-QE}, we show in Fig. 5 the complete set of SSM-inel results for all kinematics where

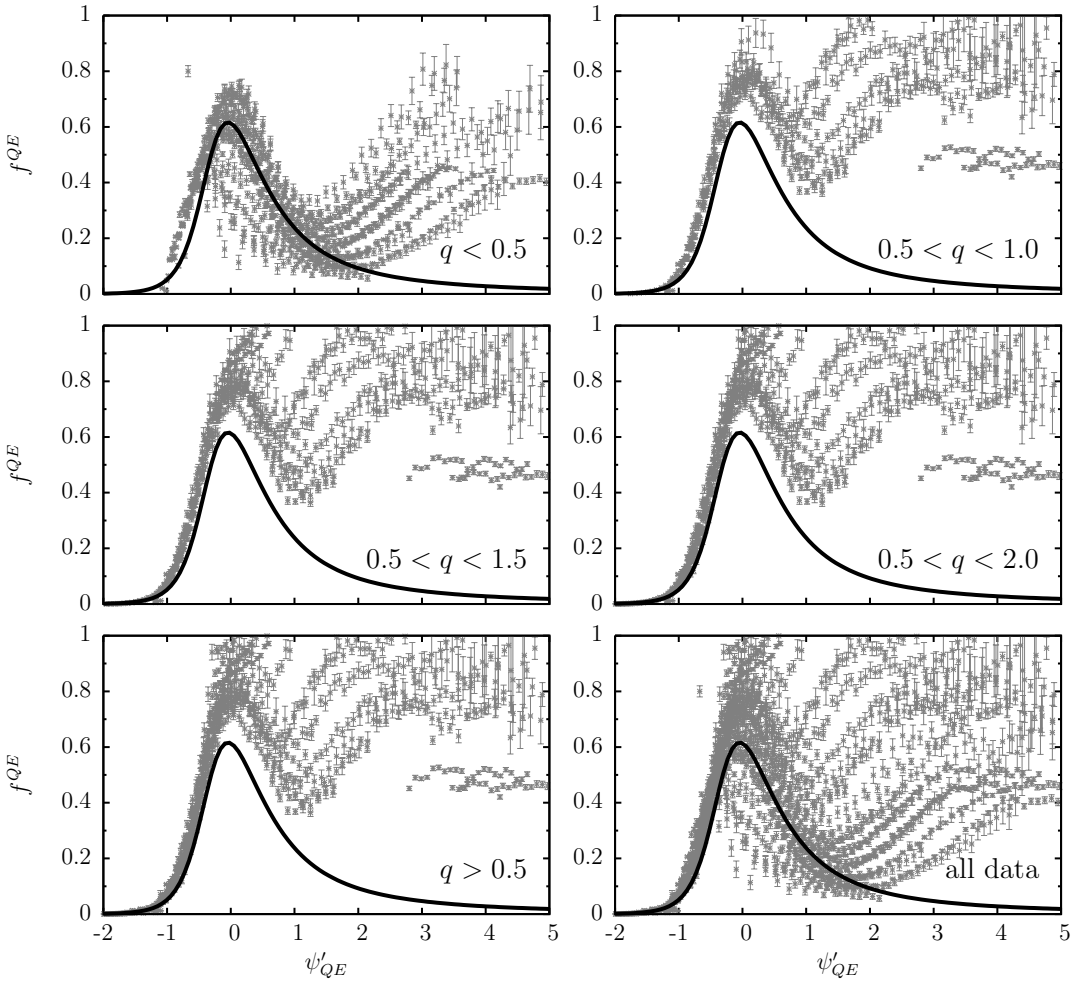

FIG. 6: Full quasielastic scaling function f^{QE} for ^{12}C as a function of ψ'_{QE}. The same kinematical cuts as in Fig. 2 are considered, as indicated in the different panels. The solid line is the phenomenological QE fit used in this work.

data are available, with the same kinematical cuts used for the results presented in Fig. 2 (see also Table I). Also, for comparison, in Fig. 6 we show f^{QE} (Eq. (10)) as a function of ψ'_{QE}.

IV. RESIDUAL NON-IMPULSIVE CONTRIBUTIONS AND SYNTHESIS OF THE CROSS SECTION

The superscaling-based model developed in the previous sections allows one to study the behavior of the superscaling function within the context of the impulse approximation and therefore to assess the size of any potential non-impulsive contributions. In particular, it is interesting to combine the two impulsive contributions denoted SSM-QE (Sec. II A) and

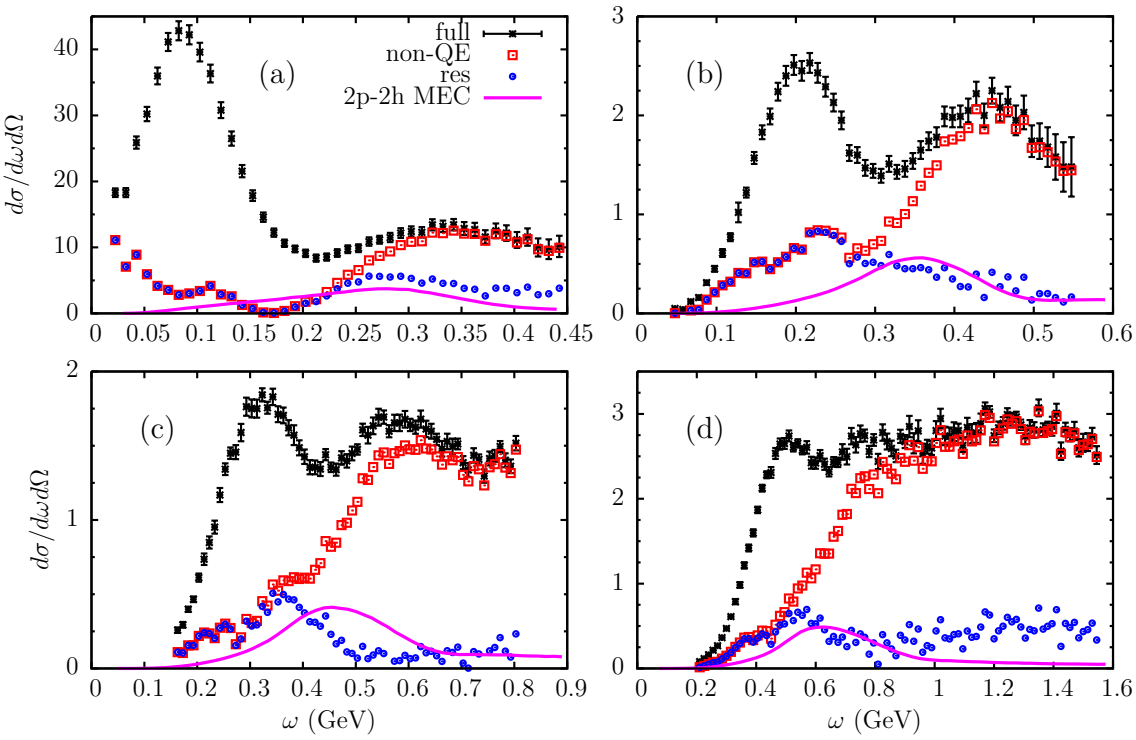

FIG. 7: (Color online) Cross sections in nb/sr/MeV versus ω. The kinematics corresponding to the various labels are the same as in Fig. 3 and Table I. The curves are discussed in the text.

SSM-inel (Sec. III A) and subtract this from the data to yield a residual:

$$\left(\frac{d\sigma}{d\epsilon' d\Omega}\right)^{res} \equiv \left(\frac{d\sigma}{d\epsilon' d\Omega}\right)^{exp} - \left(\frac{d\sigma}{d\epsilon' d\Omega}\right)^{SSM-QE} - \left(\frac{d\sigma}{d\epsilon' d\Omega}\right)^{SSM-inel} . \quad (36)$$

The results are shown in Fig. 7 for the same kinematics considered in Fig. 3. Here the (black) stars are the complete experimental data, the (red) squares the QE-subtracted cross sections [Eq. (13)] and the (blue) circles the residual cross sections [Eq. (36)]. Note that, lacking any means of evaluating what errors are incurred in the subtraction procedures, we have not given any uncertainties for the non-QE and residual cross sections shown in the figure.

Focusing on the residual cross sections we see significant contributions left over after the SSM-QE and SSM-inel results have been removed. As stated several times in the previous sections we expect there to be non-impulsive effects from 2p-2h MEC [18, 19]. Indeed, when these are compared with the residuals (shown as solid magenta curves in the figure) one sees rough agreement. That is not to say that one now has a fully satisfactory picture of inclusive electron scattering in this kinematic region — there are still several open issues. In particular, when MEC effects are included (and they are not optional; they must be included) gauge invariance requires that corresponding correlation contributions must also

occur. In [26, 27, 28, 29, 30] this problem was dealt with for the 1p-1h sector. However, this has not yet been done for the 2p-2h response, although work is in progress [51] to address this issue. Another issue goes back to comments made in the previous sections, namely, even the SSM-QE approach has some uncertainties in that scaling of the 0th kind may be broken to a small degree, and that the somewhat larger transverse scaling functions found in the RMF approach and the 1p-1h MEC contributions (which lead to a small reduction of the transverse cross section) may not completely compensate one another. In effect one could break the 0th-kind scaling by using a slightly different scaling function for the transverse contributions and thereby modify the residuals seen in the figure. It is clear, however, that a significant amount of the residual can be explained by the 2p-2h MEC contributions. In the last section we shall return to this point and comment on the implications this has for predicting neutrino reaction cross sections.

In this section we focus primarily on the cross sections and only at the end of the section we will briefly return to discuss the non-QE scaling function in order to assess the validity of SuSA-based models. Note that we should not expect the 2p-2h MEC contributions to scale using either type of scaling discussed above, *i.e.,* either the QE type or the Δ type. In fact these contributions have their own characteristic scaling behavior and work in progress is aimed at exploring this behavior in the residual data. With these comments in mind, let us work in the opposite direction and, rather than analyzing the cross section, attempt to synthesize it using the three types of contributions.

In Fig. 8 we show the net result of adding together the SSM-QE, the SSM-inel and the 2p-2h MEC contributions for comparison with the data. The results are quite encouraging: the basic qualitative structure of the data is also present in the net result of the superscaling analysis, although clearly there is more to be done before one can claim to have a fully quantitative description of inclusive electron scattering in this region of kinematics. In particular, the net result of adding the three contributions falls short of the data in the QE peak region, and this might be fixed by slightly breaking the 0th-kind scaling (as discussed above) or by exploiting the flexibility that is inevitably present in the modeling of the 2p-2h MEC contributions (for instance, by using a different shift energy than the one that was chosen for the results presented here). It should be stressed that this rather good level of agreement between theory and experiment has been obtained by adding together three separate contributions, each with its own distinctive kinematic dependence, and thus any

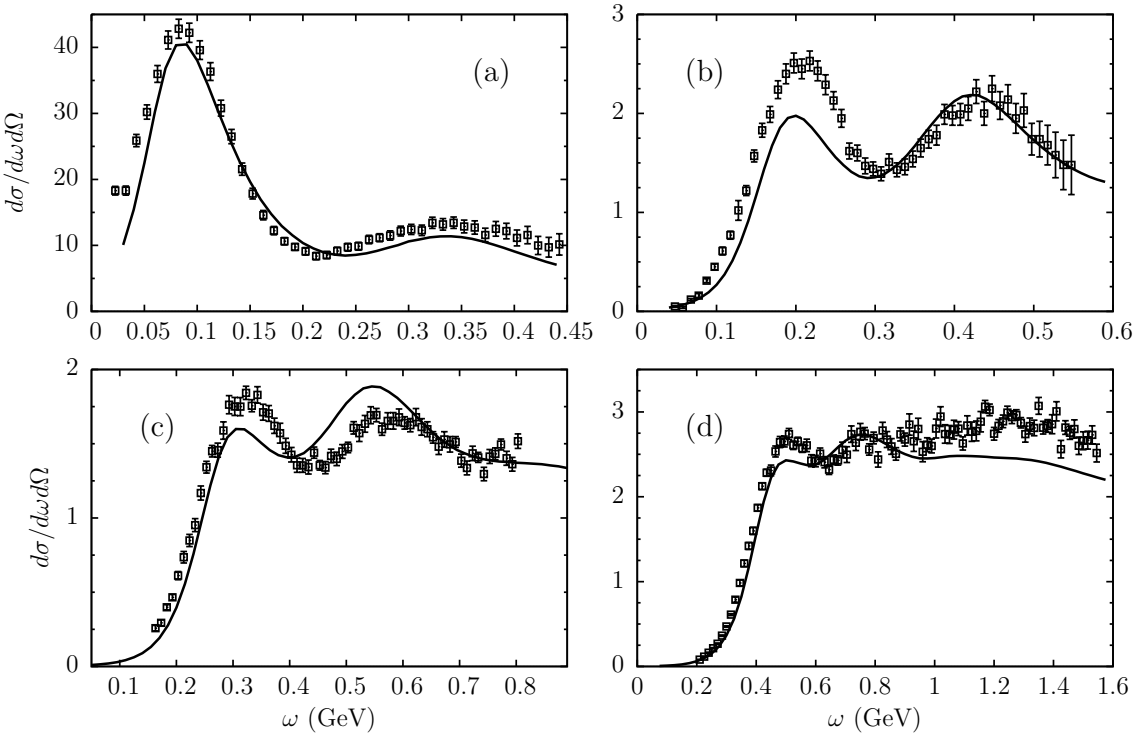

FIG. 8: Cross sections in nb/sr/MeV versus ω. The kinematics corresponding to the various labels are the same as in Fig. 3 and Table I. The curves are the sum of the SSM-QE, SSM-inel and 2p-2h MEC contributions.

attempt to represent experimental data using only a subset of the contributions is bound to fail for some choice of kinematics.

In order to make contact with the Superscaling Analysis of [7], we conclude this section by taking the non-QE superscaling functions obtained by using the sum of SSM-inel and 2p-2h MEC cross sections and inserting them in Eq. (25). These are shown in Fig. 9, for the kinematics considered in the previous figures (see Table I). The point of doing this, despite the concluding statements made in the preceding paragraph, is to provide a comparison with the phenomenological SuSA results discussed in Sec. II B. We observe that the inclusion of 2p-2h MEC contributions brings the calculated non-QE scaling function closer to the phenomenological fit, supporting the validity of the SuSA-based model for lepton-nucleus cross sections at kinematics dominated by Δ excitation. However, the strength shown by the residual data close to the QE peak, not accounted for by the theoretical MEC curves considered in this section (as discussed above), affects the non-QE scaling functions at ψ'_Δ values below approximately -1.5. This can be seen by examining the right-hand column of Fig. 3, for instance. These effects should be carefully considered in the future when constructing quantitatively reliable models.

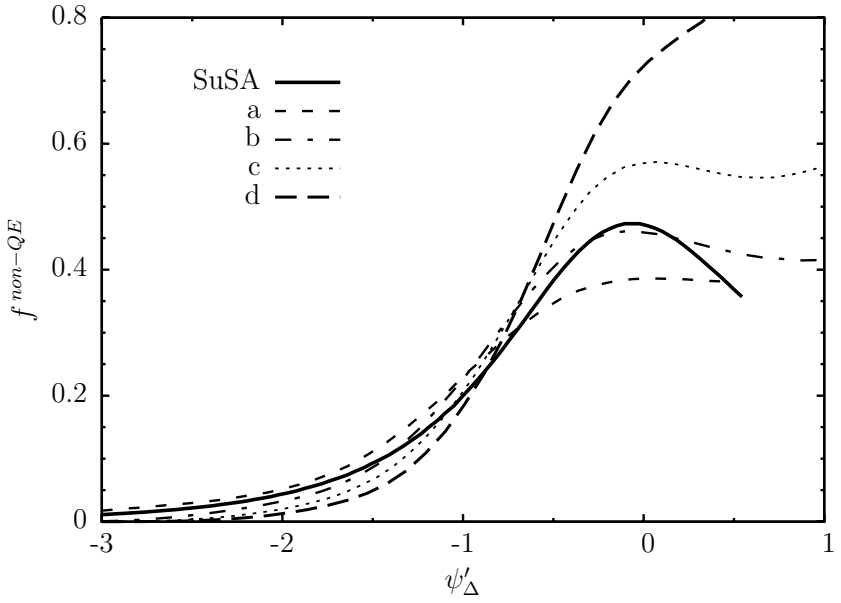

FIG. 9: Non-QE superscaling functions calculated by using the sum of SSM-inel and 2p-2h MEC contributions to the cross sections in Eq. (25). Labels a, b, c, d correspond to the kinematics used in Fig. 3 and listed in Table I. The solid line is the SuSA fit.

V. SUMMARY AND CONCLUSIONS

In this work we have explored superscaling in electron-nucleus scattering. We have started by reviewing the procedures for analyzing scaling in the quasielastic region. A universal longitudinal QE scaling function emerges, both based on phenomenology and on modeling. Upon assuming that 0th-kind scaling is satisfied (universality of transverse and longitudinal scaling functions) we arrive at our model, denoted SSM-QE, for these contributions.

Next we have focused on the region lying to the right of the QE peak, first introducing the definition of the experimental scaling function in this region, f^{non-QE}. This entails subtracting the SSM-QE scaling predictions from the data. We have studied the scaling behavior of f^{non-QE} by analyzing all available high-quality data for ^{12}C. We have found reasonable scaling below the Δ peak, with scaling violations that can be mainly explained in terms of contributions coming from higher resonances. Following the SuSA approach presented in [7], we have obtained a phenomenological fit, f^{non-QE}_{SuSA}, which differs from the phenomenological function f^{SSM-QE} obtained in previous studies of QE scattering.

In order to understand this difference, and to explore in detail the breaking of scaling shown by f^{non-QE}, we have developed an extension for inelastic electron-nucleus scattering

within the impulse approximation denoted $f^{SSM-inel}$ which is based on previous studies of the same type [6]. The model begins with the formulation of the response functions in the RFG model, and extends the latter by incorporating in them the universal scaling function f^{SSM} obtained from fits of QE scattering data, making the approach in a sense super-universal. The entire inelastic response on the nucleon is incorporated using a recent representation of the nucleon's structure functions for kinematics going from pion-production threshold to where DIS takes over [50], both for the proton [46] and neutron [47].

The comparison of this impulsive model with the experimental data, for both cross sections and non-QE scaling functions, is good, but not entirely satisfactory at first glance, since the results always fall below the data. However, the acceptable agreement of the shape of the calculated scaling function with the data, suggests that the differences between the experimental scaling functions obtained in the QE and Δ regions could be mainly explained in terms of the kinematical effects discussed in the Appendix. Additionally, the results of the SSM-inel model allow us to conclude that the scaling violations observed for $-1 < \psi'_{\Delta} < 0$ can be mostly explained by the presence of contributions from higher resonances. In particular, by comparing results from the full SSM-inel model, in which the entire inelastic responses of the nucleons are included, with a variant of this approach (denoted SSM-Δ), in which only the Δ is included, it has been possible to gain some insight into the roles played by excitations lying above the Δ.

Having explored the superscaling properties of the SSM-QE/SSM-inel model, we have used this model to subtract from the experimental data both the QE contributions and those inelastic contributions that can be described within the impulse approximation, thus isolating non-impulsive contributions. When this residual is compared with the known non-impulsive contributions, namely, those arising from 2p-2h MEC, one sees improved agreement between modeling and data. Indeed, it appears that the 2p-2h MEC contributions are essential if one is to have a quantitative picture of inclusive electron scattering at the kinematics considered in this work.

Finally, a few words are in order concerning the implications the present study has for predictions of neutrino reaction cross sections. Clearly all of the ingredients discussed here (QE, inelastic and MEC contributions) also enter in studying the latter, insofar as the vector current is concerned. The axial-vector current required for neutrino reactions is another matter, however. Unlike the polar-vector current where the leading-order MEC

effects enter as transverse effects, but not as longitudinal effects, the axial-vector current is the opposite (due to the extra γ_5 in the basic current, which switches the contributions of the upper and lower components in the required matrix elements). Accordingly, for the axial-vector currents there are no leading-order transverse effects from MEC, while there are for the axial longitudinal/charge currents. The latter are small for neutrino reactions at the kinematics of interest in this work and consequently for neutrino reactions the MEC effects enter asymmetrically — essentially, only via the polar-vector currents, but not the axial-vector currents. We have seen that the (vector) MEC effects are significant and thus any model that does not have them runs the risk of incurring errors of typically 10–20% in predicting neutrino cross sections. Using overly simple models such as the RFG is adequate for crude estimates of the neutrino cross sections, although almost certainly the SSM analyses presented here are considerably better as they capture much of the correct kinematical dependences of the polar-vector parts of the electroweak nuclear response. However, as we have seen in the present work these impulsive superscaling models do not entirely capture all of the necessary content in the currents since they are missing the non-impulsive MEC contributions. To the degree that the latter are important one has a complicated problem containing at least three parts, the SSM-QE and SSM-inel impulsive contributions together with the 2p-2h MEC effects, each with its own distinctive kinematic dependences.

Acknowledgments

We are grateful to P. Bosted for providing the code containing the new nucleon structure function parametrizations and to A. De Pace for providing the 2p-2h MEC results shown in Sec. IV. This work was partially supported by DGI (Spain): FIS2008-01143, FPA2006-13807-C02-01, FIS2008-04189, by the Junta de Andalucía, by the INFN-MEC collaboration agreement (project "Study of relativistic dynamics in neutrino and electron scattering") and by the Spanish Consolider-Ingenio 2000 program CPAN (CSD2007-00042). It was also supported in part (TWD) by the U.S. Department of Energy under contract No. DE-FG02-94ER40818.

APPENDIX: THE Δ SUPERSCALING FUNCTION AT THE Δ PEAK

In Sec. III B we observed that at the Δ peak the scaling violations shown by the superscaling function obtained within the SSM-inel model seem to be larger than those present in the data. Comparable scale-breaking effects are also obtained within the SSM-Δ model, which includes only the excitation of the Δ resonance, and therefore they cannot be explained in terms of an incorrect treatment of higher resonances. Here we show that the origin of these scaling violations in our models is related to kinematical effects and to the shape and value of the phenomenological QE function used as input at its peak. In order to do so, we work within the SSM-Δ model, whose simplicity allows us to explore in detail the effects of the various terms entering the formulae for the response functions and of the corresponding integration limits.

Let us return to the lower panel of Fig. 4, where we observe excellent scaling for $\psi'_\Delta \leq -0.5$, whereas a significant amount of scaling violation remains at larger ψ'_Δ and it increases approaching the peak.

In order to understand this behavior let us examine the integral in Eq. (33) together with the formulae presented in Sec. II B. We can easily see that, except for minor effects due to a residual μ_X dependence in the coefficients multiplying the form factors in Eqs. (19,20), the SSM-Δ superscaling function f^Δ is essentially given by the integral

$$f^\Delta_{appx}(\psi_\Delta) \equiv \int_{\mu_1}^{\mu_2} \frac{1}{\pi} \frac{\Gamma(\mu_X)/2m_N}{(\mu_X - \mu_\Delta)^2 + \Gamma(\mu_X)^2/4m_N^2} f^{SSM}(\psi_X) d\mu_X \,, \tag{A.1}$$

whose calculation indeed produces curves that are close to the full f^Δ and have the same scaling properties. We can thus use the simpler expression in Eq. (A.1) to investigate further the origin of the scaling behavior of f^Δ and the scaling violations it exhibits at the Δ peak. To do so we choose two fixed values of ψ_Δ (for simplicity we also set $E_{shift} = 0$), namely $\psi_\Delta = 0$ (*i.e.,* the Delta peak) and $\psi_\Delta = -0.5$ and look at the behavior of the integrand of Eq. (A.1). This integrand is displayed in the upper panels of Figs. 10 and 11, for $\psi_\Delta = 0$ and -0.5, respectively, for different values of the momentum transfer q, as indicated by the labels. The asterisk close to origin of the x-axis indicates the integration limit related to pion-threshold, while the different dots on the x-axis indicate the upper limit of integration. For the largest values of q considered here the latter falls outside the plotted range of μ_X and therefore the corresponding dots do not appear in the figures.

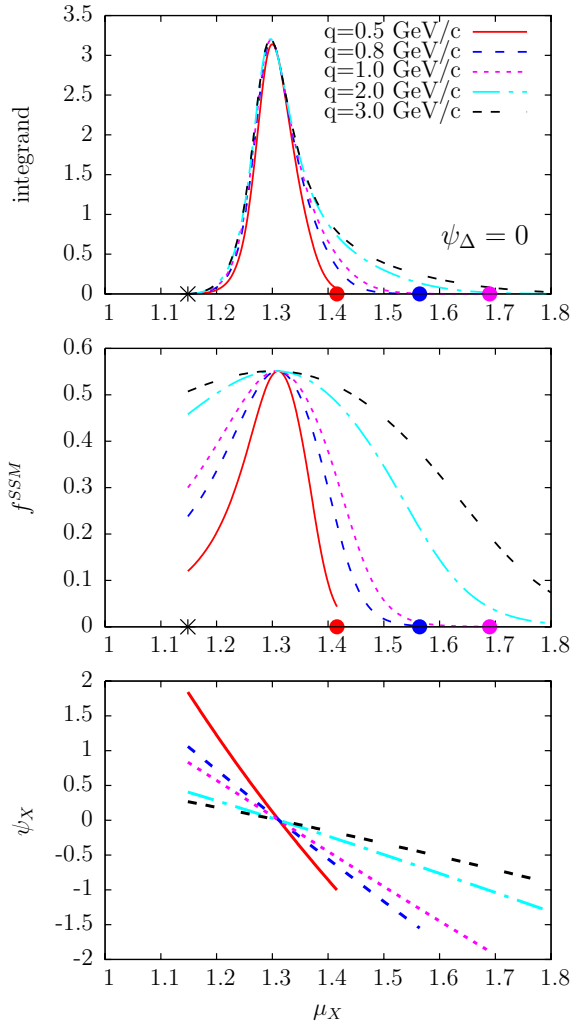

FIG. 10: (Color online) Upper panel: integrand of Eq. (A.1), *i.e.*, of f^{Δ}_{appx}, as a function of μ_X, for various values of the momentum transfer, as indicated by the labels. The asterisk and points on the x-axis indicate the lower and upper limits of integration, respectively. Middle panel: function f^{SSM} as a function of μ_X. Lower panel: inelastic scaling variable ψ_X as a function of μ_X. All curves are calculated at fixed $\psi_\Delta = 0$ (here, for simplicity, E_{shift} has been taken to be zero).

In the middle panels of the same figures we show f^{SSM} as a function of μ_X and in the lower panels we show how ψ_X varies with μ_X for fixed ψ_Δ. Note that ψ_X decreases for increasing μ_X. By looking at Fig. 10 we can see that as q increases, the dependence of ψ_X on μ_X becomes weaker and thus ψ_X stays closer to the fixed value of ψ_Δ, which in this case is 0. This means that for larger q the integrand receives contributions mostly from $f^{SSM}(\psi_X)$

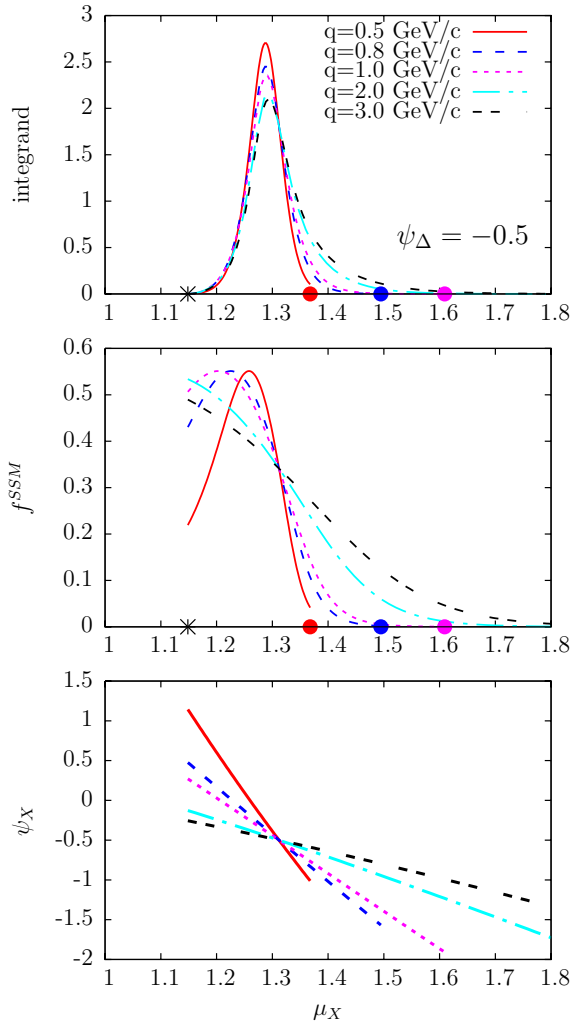

FIG. 11: (Color online) As for Fig. 10, but now at fixed $\psi_\Delta = -0.5$.

close to its peak, while for smaller q a more extended range of ψ_X values contributes. For this reason the integrand turns out to be larger for the highest values of q and this gives rise to the behavior observed in Fig. 4.

The same type of behavior of $\psi_X(\mu_X)$ is observed also for $\psi_\Delta = -0.5$ (lower panel of Fig. 11), implying that for high q the variable ψ_X stays close to the negative value -0.5, thus remaining in the region where $f^{SSM}(\psi_X)$ is small. In this case, however, this is compensated by a larger (with respect to what occurs for smaller values of q) integration interval and thus the values of f^{Δ}_{appx} for different q are very close to each other. Moving to even more negative values of ψ_Δ one could see that the larger integration interval occurring for high q is no

longer able to compensate for the smaller values of $f^{SSM}(\psi_X)$ involved in the integration, so that the larger q becomes, the smaller is the value of f^{Δ}_{appx} obtained.

Similar considerations could be applied to the integral in Eq. (28) entering in the SSM-inel model, although in this case a direct comparison between f^{Δ} and f^{Δ}_{appx} cannot be made, because of the different single-nucleon ingredients entering the cross section and the dividing factor S^{Δ} of Eq. (26), which defines f^{Δ}. In particular in this case stronger scaling violations appear even in the negative ψ'_{Δ}-region, which, as discussed in the paper, are related to the presence of higher resonance contributions in the inelastic single-nucleon structure functions.

---

[1] G. B. West, Phys. Rept. **18**, 263 (1975).

[2] D. B. Day, J. S. McCarthy, T. W. Donnelly and I. Sick, Ann. Rev. Nucl. Part. Sci. **40**, 357 (1990).

[3] T.W. Donnelly and I. Sick, Phys. Rev. Lett. **82**, 3212 (1999).

[4] T.W. Donnelly and I. Sick, Phys. Rev. C **60**, 065502 (1999);

[5] C. Maieron, T.W. Donnelly and I. Sick, Phys. Rev. C **65**, 025502 (2002).

[6] M. B. Barbaro, J. A. Caballero, T. W. Donnelly and C. Maieron, Phys. Rev. C **69**, 035502 (2004).

[7] J. E. Amaro, M. B. Barbaro, J. A. Caballero, T. W. Donnelly, A. Molinari and I. Sick, Phys. Rev. C **71**, 015501 (2005).

[8] J. E. Amaro, M. B. Barbaro, J. A. Caballero and T. W. Donnelly, Phys. Rev. Lett. **98**, 242501 (2007).

[9] J. E. Amaro, M. B. Barbaro, J. A. Caballero, T. W. Donnelly and C. Maieron, Phys. Rev. C **71**, 065501 (2005).

[10] J. A. Caballero, J. E. Amaro, M. B. Barbaro, T. W. Donnelly, C. Maieron and J. M. Udias, Phys. Rev. Lett. **95**, 252502 (2005).

[11] J. A. Caballero, Phys. Rev. C **74**, 015502 (2006).

[12] J. E. Amaro, M. B. Barbaro, J. A. Caballero, T. W. Donnelly and J. M. Udias, Phys. Rev. C **75**, 034613 (2007).

[13] J. A. Caballero, J. E. Amaro, M. B. Barbaro, T. W. Donnelly and J. M. Udias, Phys. Lett. B **653**, 366 (2007).

[14] M. Martini, G. Co', M. Anguiano and A. M. Lallena, Phys. Rev. C **75**, 034604 (2007).

[15] A. N. Antonov, M. K. Gaidarov, D. N. Kadrev, M. V. Ivanov, E. Moya de Guerra and J. M. Udias, Phys. Rev. C **69**, 044321 (2004).

[16] A. N. Antonov, M. V. Ivanov, M. K. Gaidarov, E. Moya de Guerra, P. Sarriguren and J. M. Udias, Phys. Rev. C **73**, 047302 (2006) [Erratum-ibid. C **73**, 059901 (2006)]

[17] A. N. Antonov, M. V. Ivanov, M. K. Gaidarov and E. Moya de Guerra, Phys. Rev. C **75**, 034319 (2007).

[18] A. De Pace, M. Nardi, W. M. Alberico, T. W. Donnelly and A. Molinari, Nucl. Phys. A **726**, 303 (2003).

[19] A. De Pace, M. Nardi, W. M. Alberico, T. W. Donnelly and A. Molinari, Nucl. Phys. A **741**, 249 (2004).

[20] M. V. Ivanov, M. B. Barbaro, J. A. Caballero, A. N. Antonov, E. Moya de Guerra and M. K. Gaidarov, Phys. Rev. C **77**, 034612 (2008).

[21] C. Praet, O. Lalakulich, N. Jachowicz and J. Ryckebusch, arXiv:0804.2750 [nucl-th].

[22] J. E. Amaro, M. B. Barbaro, J. A. Caballero and T. W. Donnelly, Phys. Rev. C **73**, 035503 (2006).

[23] A. N. Antonov, M. V. Ivanov, M. B. Barbaro, J. A. Caballero, E. Moya de Guerra and M. K. Gaidarov, Phys. Rev. C **75**, 064617 (2007).

[24] M. C. Martinez, J. A. Caballero, T. W. Donnelly and J. M. Udias, Phys. Rev. C **77**, 064604 (2008). M. C. Martinez, J. A. Caballero, T. W. Donnelly and J. M. Udias, Phys. Rev. Lett. **100**, 052502 (2008).

[25] L. Alvarez-Ruso, M. B. Barbaro, T. W. Donnelly and A. Molinari, Nucl. Phys. A **724**, 157 (2003).

[26] W. M. Alberico, T. W. Donnelly and A. Molinari, Nucl. Phys. A **512**, 541 (1990).

[27] J. E. Amaro, M. B. Barbaro, J. A. Caballero, T. W. Donnelly and A. Molinari, Nucl. Phys. A **697**, 388 (2002).

[28] J. E. Amaro, M. B. Barbaro, J. A. Caballero, T. W. Donnelly and A. Molinari, Phys. Rept. **368**, 317 (2002).

[29] J. E. Amaro, M. B. Barbaro, J. A. Caballero, T. W. Donnelly and A. Molinari, Nucl. Phys. A **723**, 181 (2003).

[30] J. E. Amaro, M. B. Barbaro, J. A. Caballero, T. W. Donnelly, C. Maieron and J. M. Udias,

arXiv:0906.5598 [nucl-th].

[31] M. B. Barbaro, R. Cenni, T. W. Donnelly and A. Molinari, Phys. Rev. C **78**, 024602 (2008).

[32] J. E. Amaro, M. B. Barbaro, J. A. Caballero, T. W. Donnelly and A. Molinari, Nucl. Phys. A **657**, 161 (1999).

[33] R. R. Whitney, I. Sick, J. R. Ficenec, R. D. Kephart and W. P. Trower, Phys. Rev. C **9**, 2230 (1974).

[34] P. Barreau *et al.*, Nucl. Phys. A **402** (1983) 515.

[35] R. M. Sealock *et al.*, Phys. Rev. Lett. **62** (1989) 1350.

[36] D. B. Day *et al.*, Phys. Rev. C **48**, 1849 (1993).

[37] J. S. O'Connell *et al.*, Phys. Rev. C **35**, 1063 (1987).

[38] D. T. Baran *et al.*, Phys. Rev. Lett. **61**, 400 (1988).

[39] J. Arrington *et al.*, Phys. Rev. C **53**, 2248 (1996).

[40] J. Arrington *et al.*, Phys. Rev. Lett. **82**, 2056 (1999)

[41] O. Benhar, D. day and I. Sick, Rev. Mod. Phys. **80**, 189 (2008).

[42] see also `http://faculty.virgina.edu/qes-archive`.

[43] A. Bodek and J. L. Ritchie, Phys. Rev. D **23**, 1070 (1981); Phys. Rev. D **24**, 1400 (1981). A. Bodek *et al.*, Phys. Rev. D **20**, 1471 (1979).

[44] O. Lalakulich and E. A. Paschos, Phys. Rev. D **71**, 074003 (2005).

[45] O. Benhar and D. Meloni, Nucl. Phys. A **789**, 379 (2007).

[46] P. E. Bosted and M. E. Christy, Phys. Rev. C **77**, 065206 (2008).

[47] M. E. Christy and P. E. Bosted, arXiv:0712.3731 [hep-ph].

[48] P. E. Bosted *et al.* [CLAS Collaboration], Phys. Rev. C **78**, 015202 (2008).

[49] A. Psaker, W. Melnitchouk, M. E. Christy and C. Keppel, Phys. Rev. C **78**, 025206 (2008).

[50] P. Bosted, private communication.

[51] A. De Pace, M. Nardi, W. M. Alberico, T. W. Donnelly and A. Molinari, work in progress.